Magnesium Technology 2011
Edited by: Wim H. Sillekens, Sean R. Agnew, Neale R. Neelameggham, and Suveen N. Mathaudhu
TMS (The Minerals, Metals & Materials Society), 2011

THE SOLIDIFICATION MICROSTRUCTURE AND PRECIPITATION INVESTIGATION OF MAGNESIUM-RICH ALLOYS CONTAINING Zn AND Ce

Chuan Zhang[1], Alan A. Luo[2], Y., Austin Chang[1]
[1]Department of Materials Science and Engineering, University of Wisconsin-Madison, 1509 University Avenue, Madison, WI 53706, USA
[2]Chemical Sciences and Materials Systems Lab, General Motors Global Research & Development, 30500 Mound Road, Warren, MI 48090-9055, USA

Keywords: Magnesium alloys, Mg-Zn-Ce, Phase diagram, Precipitation, Solidification

Abstract

Mg-Zn-Ce system has been identified as the alloy system for high-ductility wrought magnesium alloy development for automotive applications. The solidification microstructure and precipitation of Mg-Zn-Ce alloys were investigated to understand the phase equilibria and strengthening phases in this alloy system. The characterized microstructures of four directionally solidified Mg-Zn-Ce alloys agree well with the calculated solidification paths using computational thermodynamics coupled with the Scheil model. The precipitation of Mg_7Zn_3 intermetallic phase upon heat treatment was characterized using high-resolution transmission electron microcopy (HRTEM), a potential strengthening mechanism which will be explored in future research.

Introduction

Magnesium alloys with their weight saving advantages have been gradually accepted in automotive applications for vehicle lightweighting and environmental protection [1-4]. However, the relatively poorer mechanical properties of magnesium alloys compared to steel and aluminum alloys have limited their applications in critical structural subsystems. Recently, significant efforts have been made to develop high-strength and high-ductility magnesium alloys for automotive structural applications. It is well known that Zn is a major alloying element in magnesium alloys and is often used to improve the mechanical properties by solid solution strengthening and age-hardening. Zinc also helps overcome the harmful corrosive effect of iron and nickel impurities in the alloys [5]. However, the binary Mg-Zn alloys have some issues such as brittleness and coarse grains [6]. Therefore, binary Mg-Zn alloys are always modified by further alloying elements, such as Zr and/or rare earth (RE), in commercial alloys. RE elements have been used in magnesium alloys for many years and usually in the form of misch-metal (MM). Their strong influence on the creep resistance of Mg alloys is due to the strengthening of the α(Mg) matrix by solid solution and/or precipitation of RE-containing phases. There has been some reported work on the precipitation, morphology, structure and thermal stability of RE-containing intermetallic phases [7-9]. For better understanding the microstructure of Mg-Zn-RE alloys and subsequently enhancing their properties, the phase equilibria and thermodynamic properties of key sub-systems in the Mg-rich region, such as Mg-Zn-Ce, are of fundamental importance. Recently, the thermodynamic description of the Mg-Zn-Ce system at the Mg-rich region was reported [10].

In this paper, the solidification paths of four Mg-Zn-Ce ternary alloys were calculated using the thermodynamic description obtained by Chiu et al. [10] and Pandat [11]. Directional solidification technique was then employed to experimentally investigate the effect of Zn and/or Ce additions on the solidified microstructure of Mg-Zn-Ce alloys and validate the thermodynamic calculations. Solution and aging treatments were also carried out on one Mg-Zn-Ce alloy, and transmission electron microscopy (TEM) work was performed on the heat treated alloy to investigate the precipitating phases.

Experimental Procedure

Commercially pure magnesium and zinc, and Mg-26%Ce master alloy ingots were used to make the Mg-Zn-Ce (ZE) alloy compositions shown in Table I. The ZE alloys were prepared and melted in a 200 lb steel crucible under SF_6/CO_2 protection. The cast alloy was then cut into small pieces of about 50 g and was used for directional solidification experiment [12-14]. The axial temperature gradient was maintained at 4°C/mm in the furnace by three independently controlled heating coils. The sample was directionally solidified as cylindrical rods in a steel tube, by moving the tube downward in the furnace at 30 μm/s for about 100 mm in length. To study the precipitation microstructure, alloy samples were sealed in a quartz tube and back-filled with high-purity argon (>99.999%) atmosphere for solution treatment at 450°C for 24 h, followed by quenching into hot water. The samples were subsequently aged at 250°C for about 200 h. The X-ray diffraction (XRD), scanning electron microscopy (SEM) and High Resolution Transmission electron microscopy (HRTEM) were used for characterizations of the directionally solidified and heat-treated samples.

Table I. Alloy composition and Scheil calculated fraction of solid phase.

Alloy #	Alloy Designation	Scheil calculated solid phase fractions			
		α(Mg) %	$Ce(Mg,Zn)_{12}$ %	Mg_7Zn_3 %	MgZn %
1	Mg-2Zn-0.2Ce	97.98	0.4	1.5	0.05
2	Mg-6Zn-0.2Ce	93.60	0.47	5.7	0.2
3	Mg-2Zn-1Ce	97.19	1.79	0.98	0.3
4	Mg-7Zn-1Ce	91.48	2.28	6.02	0.2

Results and Discussion

Thermodynamic Calculations

Figure 1(a) shows the calculated liquidus projection of the Mg-Zn-Ce system in the Mg-rich corner with the compositions of Zn and Ce varying from 0 to 50%. All the alloy compositions in this paper are given in wt.% unless noted otherwise. The solidification paths of four Mg-Zn-Ce alloys were also shown in the same diagram, and they were calculated using the Scheil model, which is based on the assumptions of complete mixing in the liquid but no diffusion in the solid. As shown in this diagram, black lines are the monovariant liquidus lines and the arrows on the monovariant liquidus lines indicate the directions of decreasing temperature. The monovariant liquidus line at the Mg-rich corner is in equilibrium with the α(Mg) and $Ce(Mg,Zn)_{12}$. It should be emphasized that the $Ce(Mg,Zn)_{12}$ is a Ce-Mg binary phase with a large solid solubility of Zn extending into the Mg-Zn-Ce ternary system [10]. As can be seen from Figure 1(a), the solidification path of Alloy 1 is as follows.

$L \rightarrow L + \alpha(Mg)$ (643°C) $\rightarrow L + \alpha(Mg) + Ce(Mg,Zn)_{12}$ (552°C) $\rightarrow L + \alpha(Mg) + T_2$ (II_2, 420°C) $\rightarrow L + T_2 + Mg_7Zn_3$ (341°C) $\rightarrow T_2 + Mg_7Zn_3 + MgZn$

The temperatures were calculated based on the thermodynamic description of Chiu et al. [10]. In order to discuss the last few solidification stages of Alloy 1 in Figure 1(a), Figure 1(b) is needed since the II_1 is in a very low Ce concentration region. Figure 1(b) shows an enlarged ordinate displaying the compositions of Ce from 0 to 0.2% and Zn from 0 to 60%. The four-phase invariant, II_2, at constant pressure is referred to as a type II invariant or reaction according to Rhines [15]. The subscript 2 indicates it is the second highest type II reaction in terms of temperature, following the notation of Chang et al. [16-18]. The sequences of phase formation of the other three alloys are identical to that of Alloy 1. The primary solidification phase of these alloys is α(Mg). After the composition of the liquid reaches the $\alpha(Mg) + Ce(Mg,Zn)_{12}$ monovariant liquidus line, the α(Mg) and $Ce(Mg,Zn)_{12}$ form simultaneously. The T_2 and Mg_7Zn_3 come out subsequently during solidification and the last liquid to solidify at ternary eutectic invariant reaction: $L \rightarrow T_2 + Mg_7Zn_3 + MgZn$. It is clear from Figure 1 that the phases formed in the interdendritic regions of the solidified Mg-Zn-Ce alloys (Zn < 10% and/or Ce < 5%) are identical, while the fraction of each phase may vary with different Zn and/or Ce concentrations.

In order to investigate the effect of various additions of Zn or Ce on the microstructure of solidified Mg-Zn-Ce alloys, the fraction of solid vs. temperature diagram of the selected four Mg-Zn-Ce Alloys was superimposed and shown in Figure 2. It indicates that the Zn addition decreases the alloy liquidus temperature. For example, the liquidus temperature of Alloy 1 with 2%Zn and 0.2%Ce is 634°C, while that of Alloy 2 containing the same amount of Ce (0.2%) but higher Zn concentration (6%) decreases to 631°C. And the same trend was also found on Alloys 3 (Mg-2Zn-1Ce) and 4 (Mg-7Zn-1Ce). Figure 2 also shows that with the addition of more Ce to the Mg-Zn-Ce alloys, the primary α(Mg) fraction decrease and more interdendritic phases formed during the solidification. Based on the Scheil calculations in this study, the primary α(Mg) fraction of Alloy 1

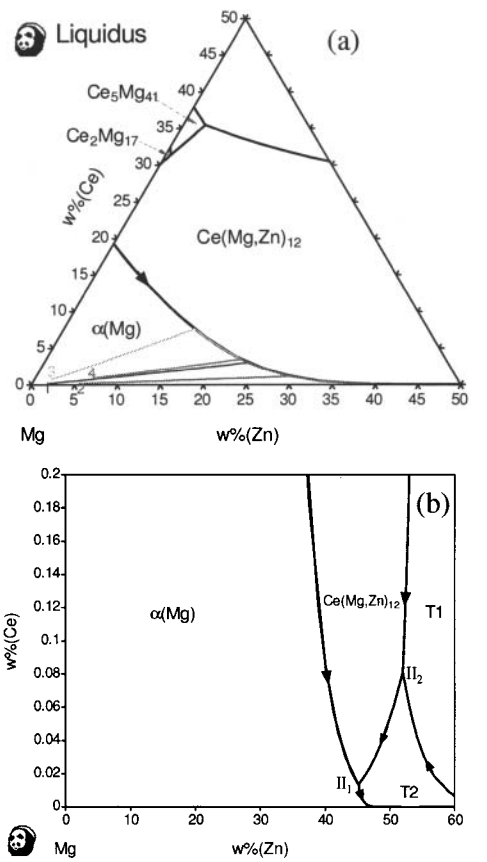

Figure 1. (a) Calculated liquidus projection of the Mg-Zn-Ce system at the Mg-rich region with the solidification path of four selected alloys using Scheil model; (b) Enlarged diagram – alloy 1: Mg-2Zn-0.2Ce; alloy 2: Mg-6Zn-0.2Ce; alloy 3: Mg-2Zn-1Ce; alloy 4: Mg-7Zn-1Ce (wt.%).

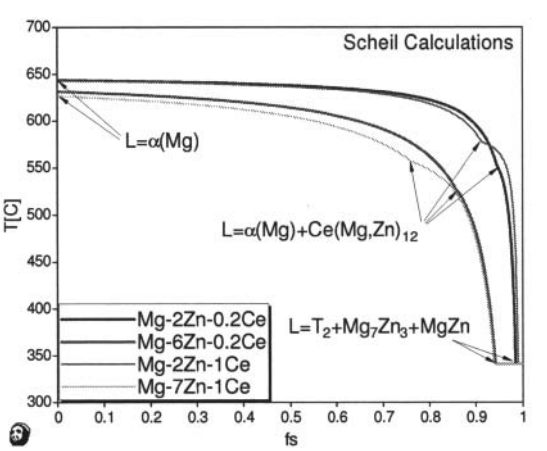

Figure 2. Fraction of solid vs. temperature diagram of four Mg-Zn-Ce alloys using Scheil model.

(Mg-2Zn-0.2Ce) is around 95%. However, the primary α(Mg) fraction of Alloy 3 (Mg-2Zn-1Ce) with higher Ce concentration is about 4% less than that of alloy 1. The Scheil calculations of the fractions of all interdendritic phases are summarized in Table I.

Solidification Microstructure

Figure 3 shows the SEM backscattered electron (BSE) images of the directionally solidified microstructure of the Mg-Zn-Ce alloys in the longitudinal direction in the steady state region. As shown in Figure 3(a), the directionally solidified Alloy 1 (Mg-2Zn-0.2Ce) shows the existence of one dominant phase with dark contrast and some regions containing devoiced eutectic-like microstructure with bright contrast. The XRD and SEM energy dispersive spectroscopic (EDS) phase identification results show that the dark matrix is α(Mg) and the bright phase is Mg_7Zn_3, which is in good agreement with the thermodynamic calculation results in Figures 1 and 2. It is not surprising that the $Ce(Mg,Zn)_{12}$ phase was not found in the solidified Alloy 1 due to its small volume fraction (<0.5%). The microstructure of Alloy 2 shown in Figure 3(b) is similar to that of Alloy 1. Two phases α(Mg) and Mg_7Zn_3 were identified. However, the fraction of Mg_7Zn_3 in the interdendritic region is more than that of Alloy 1, which is due to its higher Zn concentration and was predicted based on our Sheil calculations shown in Figure 2. The microstructure of Alloys 3 (Mg-2Zn-1Ce) and 4 (Mg-7Zn-1Ce) are shown in Figure 3 (c) and (d), respectively. For Alloy 3 shown in Figure 3(c), the XRD phase identification indicates that the dark α(Mg) coexisting with bright contrast interdendritic phases $Ce(Mg,Zn)_{12}$ and Mg_7Zn_3. However, it is very difficult to distinguish these two bight contract phases by SEM due to their similar morphology and contract within the interdendritic regions. The TEM selected area diffraction (SAD) was then carried out to confirm the existence of these two phases. The results will be reported in a future publication due to the limited space available in this paper. As shown in Figure 3(d), the microstructure of Alloy 4 (Mg-7Zn-1Ce) is similar to that of Alloy 3 (Mg-2Zn-1Ce), but the volume fraction of interdendritic phases is more due to its higher Zn concentration than that of Alloy 3. Therefore, the directional solidification results are in good agreement with the thermodynamic calculations using the Scheil model.

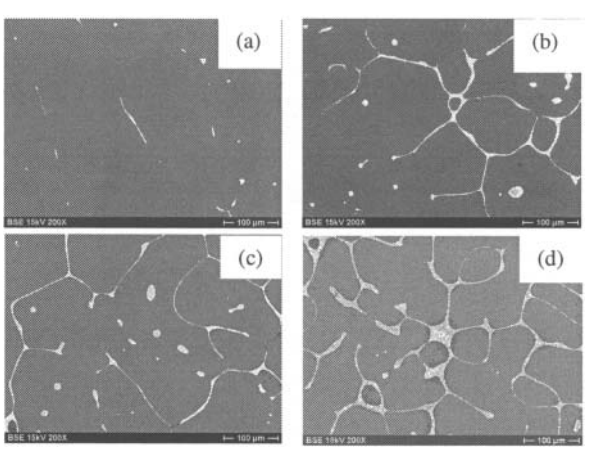

Figure 3. SEM/BSE images show the microstructure of directionally solidified Mg-Zn-Ce alloys (a) alloy 1: Mg-2Zn-0.2Ce; (b) alloy 2: Mg-6Zn-0.2Ce; (c) alloy 3: Mg-2Zn-1Ce; (d) alloy 4: Mg-7Zn-1Ce (wt.%).

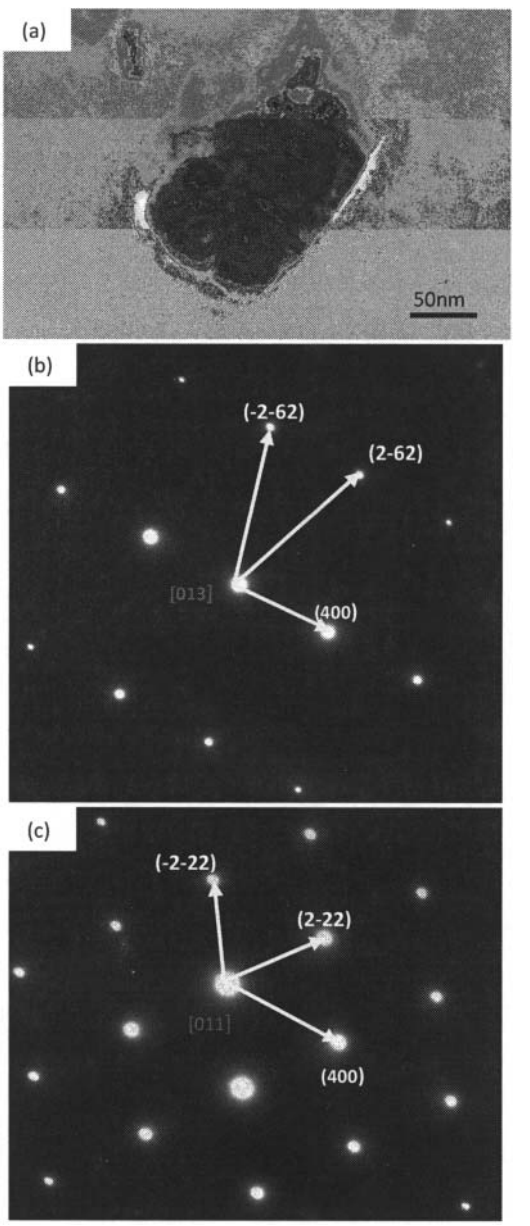

Figure 4. The TEM BF image and SAD of the Mg_7Zn_3 precipitate with α(Mg) matrix of heat treated Alloy 4 (Mg-7Zn-1Ce).

Precipitation Microstructure

Alloy 4 (Mg-7Zn-1Ce) was selected for the precipitation microstructure study due to its higher Zn and Ce concentrations. Figure 4 shows the HRTEM bright-field (BF) image and SAD of Alloy 4 (Mg-7Zn-1Ce) after solution and ageing treatments. The precipitating phase in the α(Mg) matrix was identified to be Mg_7Zn_3 by the diffraction patterns. As in many other alloy systems, the strengthening of the alloys is not only from the formation of thermodynamically stable intermetallics in the grain boundaries, but also the precipitates in the α(Mg) matrix after proper heat treatment processing. The precipitation of Mg_7Zn_3 phase in Mg-Zn-Ce alloys should be explored to improve the strength of the alloys.

Conclusions

1. The calculated solidification paths of four Mg-rich Mg-Zn-Ce alloys are in good agreement with the directional solidification microstructures of these alloys. The as-cast microstructures of four directionally solidified Mg-Zn-Ce alloys agree well with the computational thermodynamics calculations using the Scheil model.
2. Preliminary precipitation investigation found the Mg_7Zn_3 precipitation in the α(Mg) matrix after solution and age heat-treatments, indicating potential age-hardening for this alloy system, which should be explored in future research to improve the strength of the high-ductility Mg-Zn-Ce alloys.

Acknowledgements

The authors acknowledge the support of GM Global R&D, the financial support from NSF DMR No. 1005762 and Wisconsin Distinguished Professorship. Dr. Anil Sachdev of GM Global R&D is gratefully acknowledged for technical discussions.

References

1. E. Baril, P. Labelle, M.O. Pekguleryuz, "*Elevated Temperature Mg-Al-Sr: Creep Resistance, Mechanical Properties, and Microstructure*", JOM, (2003), pp. 34-39.

2. M.O. Pekguleryuz, A.A. Kaya. *In: K.U. Kainer, editor. Magnesium Alloys and their Applications.* Germany, Wiley-VCH Verlag GmbH, (2003), p. 74.

3. A.A. Luo, *"Recent magnesium alloy development for elevated temperature applications"*, Int. Mater. Rev., 49 (2004), pp. 13-29.

4. Y. Nakamura, A. Watanabe, K. Ohori, *"Effect of Ca, Sr Additions on Properties of Mg-Al Based Alloys"*, Mater Trans., 47(4) (2006), pp. 1031-1039.

5. M.M. Avedesian, H. Baker, ASM Specialty Handbook, American Society for Metals, Materials Park, OH, 1999.

6. C.J. Boehler, *"The tensile and creep behavior of Mg-Zn alloys with and without Y and Zr as ternary elements"*, J Mater Sci., 42 (2007), pp. 3675–3684.

7. I.J. Polmear, *"Recent developments in light alloys"*, Mater. Trans. JIM, 37 (1) (1996) 12.

8. L.Y. Wei, G.L. Dunlop, H. Westengen, *"Development of microstructure in cast Mg-Al-rare earth alloys"*, Mater. Sci. Technol., 12 (9) (1996) 741.

9. R. Ferro, A. Saccone, G. Borzone, *"Rare earth metals in light alloys"*, J. Rare Earths, 15 (1) (1997), pp. 45-61.

10. C.N. Chiu, J. Gröbner, A. Kozlov, R. Schmid-Fetzer, *"Experimental study and thermodynamic assessment of ternary Mg–Zn–Ce phase relations focused on Mg-rich alloys"* Intermetallics, 18(4) (2010), pp. 399-405.

11. Pandat 8.0–Phase Diagram Calculation Software for Multi-component Systems, Computherm LLC, 437 S. Yellowstone Dr., Suite217, Madison, WI, 53719, USA, 2008.

12. C. Zhang, D. Ma, K. Wu, H. Cao, J. Zhu, G. Cao, S. Kou, Y.A. Chang, in Magnesium Technology 2006 (Editors: Luo A.A., Neelameggham N.R. and Beals R.S.), TMS (The Minerals, Metals and Materials Society), 2006, p. 45.

13. C. Zhang, D. Ma, K.-S. Wu, H.-B. Cao, G.-P. Cao, S. Kou, Y. A. Chang, X-Y. Yan, *"Microstructure and microsegregation in directionally solidified Mg–4Al alloy"*, Intermetallics, 15 (2007), pp. 1395-1400.

14. C. Zhang, H.B. Cao, V. Firouzdor, S. Kou, Y.A. Chang, *"Microstructure investigations of directionally solidified Mg-rich alloys containing Al, Ca and Sn"*, Intermetallics, 18(8) (2010), pp. 1597-1602.

15. F.N. Rhines, Phase Diagrams in Metallurgy, McGraw-Hill Book Company, NY, 1956.

16. Y.A. Chang, J.P. Neumann, A. Mikula, D. Goldberg, *"Phase Diagrams and Thermodynamic Properties of Ternary Copper-Metal Systems"*, The International Copper Research Association, Inc., New York, N.Y. (1979), pp. 702.

17. Y.A. Chang, J.P. Neumann, U.V. Choudary, *"Phase Diagrams and Thermodynamic Properties of Ternary Copper-Sulfur-Metal Systems"*, The International Copper Research Association, Inc., New York, N.Y. (1979), pp. 200.

18. Y.A. Chang, K.-C. Hsieh, *"Phase Diagrams of Ternary Copper-Oxygen-Metal Systems"*, ASM International, Metals Park, Ohio, 1989.